Characteristics of dual-frequency capacitively coupled SF_6/O_2 plasma and plasma texturing of multi-crystalline silicon*

Xu Dong-Sheng(徐东升)[a], Zou Shuai(邹 帅)[a)b)], Xin Yu(辛 煜)[a)†],
Su Xiao-Dong(苏晓东)[a], and Wang Xu-Sheng(王栩生)[b)]

[a)] *Provincial Key Laboratory of Thin Films, School of Physical Science and Technology, Soochow University, Suzhou* 215006, *China*
[b)] *Canadian Solar Inc. China, Suzhou* 215000, *China*

(Received 12 November 2013; revised manuscript received 9 December 2013; published online 10 April 2014)

Due to it being environmentally friendly, much attention has been paid to the dry plasma texturing technique serving as an alternative candidate for multicrystalline silicon (mc-Si) surface texturing. In this paper, capacitively coupled plasma (CCP) driven by a dual frequency (DF) of 40.68 MHz and 13.56 MHz is first used for plasma texturing of mc-Si with SF_6/O_2 gas mixture. Using a hairpin resonant probe and optical emission techniques, DF-CCP characteristics and their influence on mc-silicon surface plasma texturing are investigated at different flow rate ratios, pressures, and radio-frequency (RF) input powers. Experimental results show that suitable plasma texturing of mc-silicon occurs only in a narrow range of plasma parameters, where electron density n_e must be larger than 6.3×10^9 cm^{-3} and the spectral intensity ratio of the F atom to that of the O atom ([F]/[O]) in the plasma must be between 0.8 and 0.3. Out of this range, no cone-like structure is formed on the mc-silicon surface. In our experiments, the lowest reflectance of about 7.3% for mc-silicon surface texturing is obtained at an [F]/[O] of 0.5 and n_e of 6.9×10^9 cm^{-3}.

Keywords: dual frequency capacitively coupled plasma, plasma texturing, multi-crystalline silicon, electron density

PACS: 52.27.Cm, 52.70.Ds, 52.70.Nc **DOI:** 10.1088/1674-1056/23/6/065201

1. Introduction

Surface texturing is important in reducing light reflection and thus improving the photoelectric conversion efficiency of silicon solar cells. A low-cost chemical wet texturing process is widely adopted in silicon solar cell surface texturing industries However, this process may bring about chemical pollution environmentally and also increase the industrial production cost of pollution treatment. In view of this issue, the dry-plasma etching technique is proposed for texturing the multi-crystalline silicon (mc-Si) solar cell due to less chemical waste, low reflection, etc.

The fluoro-based reactive plasma etching process for the mc-Si solar cell has been explored intensively.[1–3] It is well known that a cone-like surface structure, formed after texturing regardless of grain orientation of mc-Si wafer, will confine most of the incident light inside a nanometer-sized structure, thus resulting in an extremely low reflection of the silicon surface. It was reported that a solar cell was fabricated on 15×15-cm^2 mc-Si solar cells using Cl_2 plasma, with an energy conversion efficiency of $\sim$ 17%.[1–3] Ruby *et al.*[4] developed several metal-catalyst-assisted reactive ion etching (RIE)-texturing techniques using SF_6/O_2 plasma. Yoo *et al.*[5–7] used SF_6/O_2 plasma to texture mc-Si solar cells without any mask. However, in most of the work reported in the literature, few reports focus on the SF_6/O_2 plasma characteristics for silicon plasma texturing and the plasma texturing mechanism of mc-silicon.

Plasma containing SF_6 and O_2 generally has a nature of strong electronegativity, therefore, conventional Langmuir probe measurement faces a great challenge due to the presence of negative ions, probe contamination, and RF pickup in the measurement circuit, etc. Compared with the Langmuir probe, the microwave hairpin resonance probe (HRP) has been proved to be an effective diagnostic tool in measuring the electron density in reactive plasmas with low pressure.[8] The main advantage of this technique is that the floating hairpin probe avoids the influence of the outer circuit on sheath thickness, meanwhile, floating the probe makes the probe surface potential follow the plasma potential especially in RF-excited plasma.[9,10] That is, it requires no net current as opposed to the Langmuir probe,[10] which typically sweeps the probe tip bias to collect electron and ion current. The hairpin resonance probe was introduced by Stenzel[11] in 1976 to measure the electron density n_e in low pressure discharge. Later, Piejak *et al.*[12] derived a correction to the measured electron number density to account for effects resulting from the formation of the space-charge sheath surrounding the hairpin. Hebner and Abraham[13] developed a general model to account for sheaths with embedded positive and negative charges, depending on the polarity of the bias. In recent years, the hairpin probe res-

*Project supported by the Prospective Project of Industry–University–Research Institution of Jiangsu Province, China (Grant No. BY2010125) and the National Natural Science Foundation of China (Grant No. 11175127).

†Corresponding author. E-mail: xylzf_1999@suda.edu.cn

© 2014 Chinese Physical Society and IOP Publishing Ltd

onance technique has been used in the diagnostics of fluoro-based plasmas. Hebner and Abraham[14] developed this technique to identify electron and negative ion densities utilizing a hairpin resonant structure, in combination with laser photodetachment spectroscopy, in inductively coupled fluorocarbon plasma. Curley *et al*.[15] later measured electron and negative ion densities in an inductively driven plasma containing mixtures of SF_6 and Ar. Coburn and Chen[16] measured the electron density using a hairpin resonance probe and the positive ion flux with an RF-biased ion flux probe in capacitively coupled fluorocarbon plasmas.

Optical emission spectroscopy (OES) is effective as an end point detection method in the textured process. A drawback of the technique is that the gathered information comes from the excited states of the species rather than the ground state atoms or molecules. This problem can be solved using the well-known actinometry technique. In this method, the intensity of light emitted by an excited state of a species in a plasma is assumed to be proportional to its ground-state concentration.[16,17] The data are usually corrected for variation in the electron density by dividing the signal by the intensity of emission from an excited state of a noble gas (often argon) added in small quantity.[15] Actinometry has been most extensively used to monitor atomic fluorine and oxygen concentrations in fluoro-oxygen plasmas.[18–22] For F-atom actinometry, a common choice for the tracer gas is argon with a 750.4-nm actinometer line, which has a threshold energy of 13.5 eV. For F atoms, 703.7 nm is commonly chosen, with a threshold energy of 14.5 eV. For O-atom actinometry, several groups demonstrated that only 844-nm emission is considered to be the most reliable with a dissociative excitation threshold energy of 16.1 eV.[19–21]

In this paper, different from the conventional CCP driven by a single radio frequency, the CCP driven by dual frequency is first used to texture mc-Si with different discharge parameters. High frequency power with a frequency of 40.68 MHz can generate enough electron density, which may shorten the process time largely. While low frequency power with a frequency of 13.56 MHz can support suitable bombardment energy of ions incoming to the wafer surface. A self-made microwave hairpin resonance probe is adopted to monitor the plasma density in the electro-negative SF_6/O_2 plasma. The spectral lines of radicals contributed to texturing structure formation such as F and O atoms, are observed by optical emission spectroscopy. Plasma textures of mc-silicon surface with different discharge parameters are carried out in the dual-frequency excited CCP. The mc-Si surface morphology after plasma treatment is observed by the field emission scanning electron microscope (FE-SEM) technique. Then, the correlation between plasma properties and silicon texture is set up.

The rest of this paper is organized as follows. In Section 2, experimental details of the dual frequency excited CCP reactor and plasma diagnostics are described. In Section 3, experimental results and discussion are presented. Finally, some conclusions are drawn from the present study in Section 4.

2. Experimental details

The experimental setup is shown in Fig. 1(a), as described elsewhere.[23] The discharges were maintained in a stainless steel chamber between two parallel-plate stainless steel electrodes. The two electrodes were separated by 45 mm, with the upper electrode diameter being 220 mm and the lower being 250 mm. The upper water-cooled electrode was connected with the 40.68-MHz RF power source. The lower water-cooled electrode was connected with the 13.56-MHz RF power source. The matching pper and lower boxes each have a network that is an "L" type configuration comprised of two variable capacitors and a fixed inductor. The chamber wall was electrically grounded. The discharge gases (SF_6/O_2/Ar) in this experiment were introduced through mass flow controllers via a gas flow ring into the chamber. Pressure was controlled by a throttle valve together with mass flow controllers. The chamber could be pumped down to a pressure less than 5×10^{-3} Pa via a combination of turbomolecular pumping and mechanical pumping.

The probe tip was located at the radial center of the discharge chamber. A schematic drawing of the HRP head structure is shown in Fig. 1(b). The hairpin structure in this probe was made of 0.15-mm diameter tungsten wire coated with silver and had an approximate length of 20 mm, with a separation of 2.2 mm between the limbs. The hairpin was made fully floating via high temperature endured epoxy glue by physically separating the inductive loop that was formed with the center conductor (1-mm diameter) of RG223 coaxial cable, another terminal of the loop is grounded. The diameter of the inductive loop was 3.5 mm. To increase the coupling between the hairpin structure and the induction loop, a two-turn coil is used for the loop rather than a more conventional single turn loop. The separation of the induction coil from the hairpin structure plane was about 1 mm. The coaxial cable of this probe was connected to a network analyzer (Agilent N5230A) used in reflection mode in this experiment, that is, the S_{11} signal was recorded. The hairpin probe is essentially an open-ended quarter wave transmission line whose resonant frequency is related to the dielectric constant of the surrounding medium. When the probe is inserted into the plasma, the resonant frequency will offset its characteristic frequency in a vacuum. From the frequency offset, the raw electron density is determined with the frequency difference between resonances with and without plasma, as in the following equation[12]

$$n_{\mathrm{e}} = \frac{f_{\mathrm{r}}^2 - f_{\mathrm{r0}}^2}{0.81} \times 10^{10}\ (\mathrm{cm}^{-3}), \tag{1}$$

where n_e is the electron density in cm^{-3}, f_{r0} and f_r (in GHz) are the resonant frequencies in a vacuum and plasma, respectively. The plasma density corrected for the presence of a sheath may be directly expressed as[12]

$$n'_e = \frac{f_r^2 - f_{r0}^2}{0.81} \times \frac{1}{1-(f_{r0}/f_r)^2 \cdot \Lambda} \ (cm^{-3}), \tag{2}$$

where $\Lambda = \ln(b/a)/\ln(2h/a)$, a being the probe wire radius, h the distance between the axis of the probe wire and the medial plane, and $b = s + a$ the sheath outer radius, with s being the sheath width, assuming that the sheath surrounding the probe is a vacuum layer ($\varepsilon_r = 1$). The sheath width s is calculated according to the collisionless Child–Langmuir law[24]

$$s = 0.585\left(\frac{2V_0}{T_e}\right)^{3/4}\lambda_D, \tag{3}$$

where V_0 is the voltage drop in the sheath and T_e is the electronic temperature in eV. The voltage drop in the sheath is given by[24]

$$V_0 = \frac{T_e}{2}\ln\left(\frac{m_i}{2\pi m_e}\right), \tag{4}$$

where m_e is electron mass and m_i is weighted ion mass.[25]

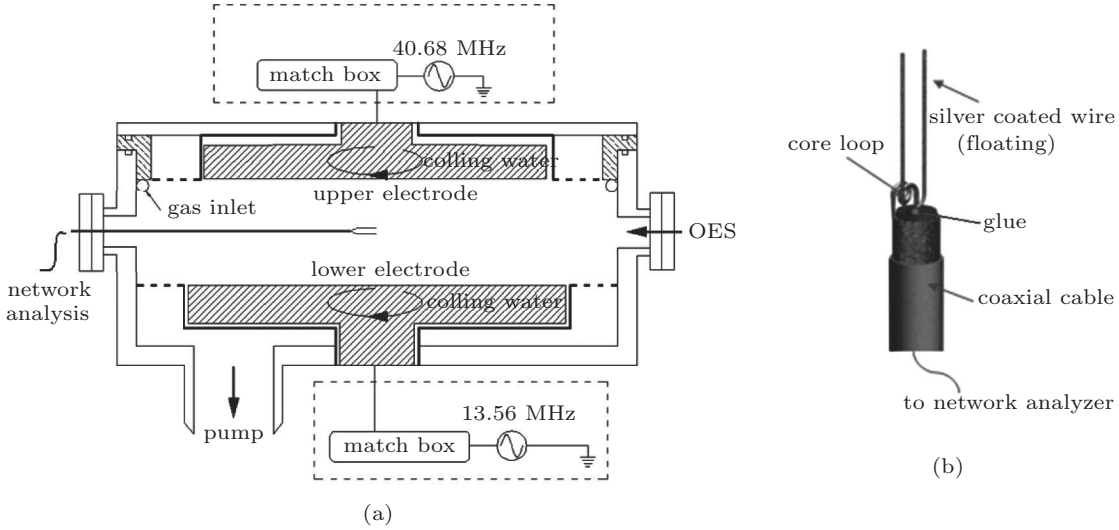


Fig. 1. Schematic diagram of (a) DF-CCP plasma and (b) hairpin resonance probe (HRP).

An optical emission spectrometer (OES, AvaSpec-2048FT-8-RM) was placed toward the opposite quartz window to measure the intensities of the interesting emission lines with different discharge parameters in the plasma discharge. The wavelength resolution of the spectrometer is 0.05 nm∼ 0.13 nm and the wavelength range is 200 nm∼ 900 nm.

In our experiments, argon concentration was chosen to be 1%∼ 5% of the feedstock gas density. In order for the actinometry technique to be successful, the emission lines under investigation were emitted from argon at 750.4 nm, fluorine at 703.7 nm, and oxygen at 844.6 nm. Figure 2 shows typical optical emission spectrum of a DF capacitively coupled SF_6/O_2 (45 sccm/5 sccm, with a trace amount of Ar) plasma.

The surface morphology of mc-Si after plasma treatment was characterized by the FE-SEM technique with the S-4700 model. The reflectance of the plasma-treated mc-Si surface was measured by a UV-VIS spectrophotometer (PV Measurements. Inc) using the integrating sphere in the range 300 nm–1200 nm.

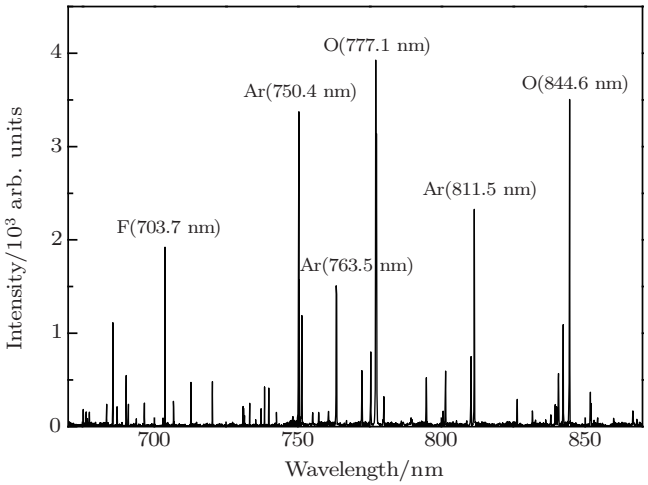


Fig. 2. A typical optical emission spectrum of $SF_6/O_2/Ar$ (45/5/1 sccm) plasma at 300 W and 7.5 mTorr. The unit 1 Torr = 1.33322×10^2 Pa.

3. Experimental results and discussion

3.1. Electron density measurements in SF_6/O_2 plasma with microwave hairpin resonance probe

Figure 3 shows the resonance absorption signal from the S_{11} channel, recorded by a network analyzer in SF_6/O_2 plasma

with different O_2 flow rates ranging from 0 sccm to 24 sccm, while the SF_6 flow rate is kept at 45 sccm and the discharge pressure is controlled at 7.5 mTorr by adjusting the butterfly valve angle as adding the O_2 flow rate. The input power applied to the upper electrode is kept at 300 W and the lower electrode is grounded. It can be seen from Fig. 3 that the resonant frequency signal presents a large offset as SF_6/O_2 plasma is onset due to the difference in dielectric constant between a vacuum and plasma. With the continuous increase of the O_2 flow rate, the resonant frequency shifts closer to the vacuum resonant frequency. This indicates a decrease in electron density with increasing the O_2 flow rate in SF_6/O_2 plasma. From formula (2), the electron density is derived as shown in the inset of Fig. 3. It can be found that the electron density experiences an abrupt decrease first from 7.5×10^9 cm^{-3} to 6.5×10^9 cm^{-3} with the O_2 flow rate decreasing from 0 to 10 sccm and then a slight decrease from 6.5×10^9 cm^{-3} to 6.2×10^9 cm^{-3} with the O_2 flow rate increasing.

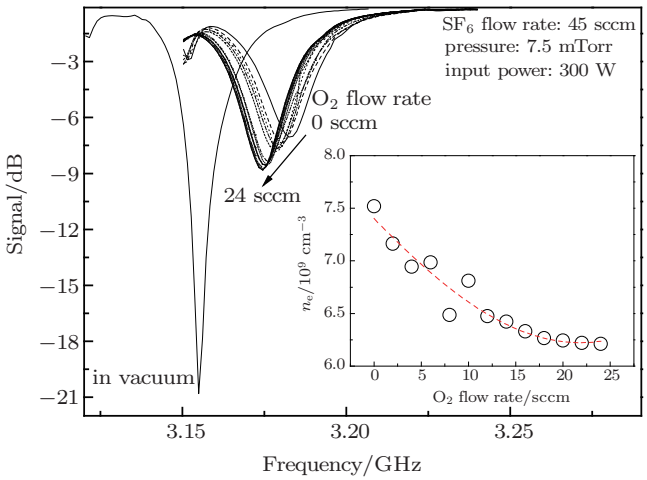


Fig. 3. (color online) Variations of absorption signal with resonant frequency at different O_2 flow rates in SF_6/O_2 discharge at 7.5 mTorr. Inset: variation in electron density of plasma as a function of the O_2 flow rate.

Figure 4 shows electron density variations with discharge pressure and upper electrode power in SF_6/O_2 (45 sccm/5 sccm) plasma. A decrease in electron density with increasing pressure is found clearly. The increase of input power leads to an increase in electron density, but the increase rate of electron density is much lower than that in electropositive plasma such as Ar.[25] The reason for this is that a certain energetic electron generated by RF heating in electronegative plasma will not only ionize the molecules or atoms, but also, most importantly, participate in dissociation, excitation and electron attachment processes via inelastic collisions in between, and the consumption of these electrons causes the electron density to stay at a lower level with increasing pressure.

13.56-MHz input power applied to the lower electrode will generate bias electric field to accelerate ions to bombard the electrode for enhancing deposition or etching effects. In our experiment, we investigate the effect of bias power on the electron density in SF_6/O_2 plasma. The other experimental conditions are the same as the experimental description in Fig. 3. Surprisingly, the resonance peak from HRP pick-up almost does not shift with bias input power increasing from 0 W to 60 W, the forming bias voltage varying from 0 V to -80 V at 60 W[25] (not shown here). This might be due to the fact that secondary electrons produced by ion bombardment induced by 13.56-MHz input power mainly participate in the dissociation or excitation process rather than the ionization process near the plasma sheath edge.

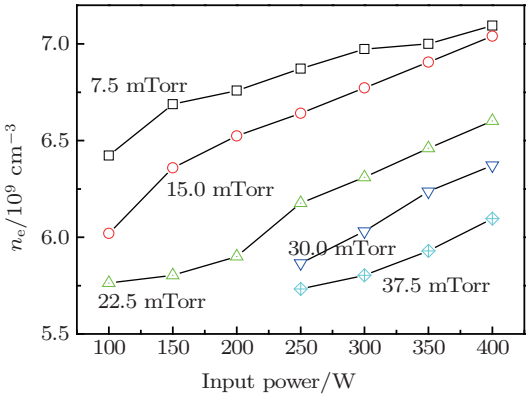


Fig. 4. (color online) Variations of electron density with pressure and upper electrode input power in SF_6/O_2 plasma with SF_6/O_2 = 45 sccm/5 sccm and grounded lower electrode.

When adding O_2 into SF_6 plasma, some reactions between their active species happen, among which a typical chemical reaction is as follows:[26]

$$O + SF_x \rightarrow SOF_{x-1} + F \quad (1 \leq x \leq 6). \tag{5}$$

Obviously, O_2 addition increases the dissociation of SF_x ($x = 1 \sim 6$) by reacting with SF_x radicals and thus preventing their recombination with fluorine to reform SF_6.[26,27] Dissociation reaction of O_2 with electrons and dissociative attachment process of electron[26] with the generated strong electronegative F atoms cause a decrease in electron density with the increase of the O_2 flow rate as shown in Fig. 3. With increasing discharge pressure, the collision rate between O and SF_x radicals increases and thus more F atoms from chemical reaction (3) are formed. These replacement reactions in combination with the dissociative attachment of electrons induce the decrease in the electron density with pressure increasing in Fig. 4.

3.2. Emission intensity of interesting radicals in SF_6/O_2 plasma by using OES technique

In the plasma containing SF_6/O_2 gases for mc-Si surface texturing, the role of F atoms detached from SF_x ($x = 1$–6) is generally to etch silicon, while the role of O atoms is to oxide silicon surface besides the collision reaction. Therefore, the

ratio between F and O atoms in the plasma will modulate the processes of surface passivation and etching and thus determine the formation of the silicon surface texturing microstructure. Therefore, it is necessary to understand the influence of discharge parameters on radical behavior in SF_6/O_2 plasma.

The ratios of I_F/I_{Ar} and I_O/I_{Ar} from the emission intensities of F (703.7 nm), O (844.6 nm), and Ar (750.4 nm) are used to estimate F and O atomic relative densities. The ratios of I_F/I_{Ar}, I_O/I_{Ar}, and I_F/I_O are plotted as a function of the O_2 flow rate in Fig. 5. The O atom relative concentration is expected to increase linearly with O_2 addition increasing, whilst the F atom relative concentration first increases with the O_2 flow rate increasing up to 6 sccm and then keeps constant basically. The reason for this may be due to the generation of energetic electro-negative F atoms caused by the collisional reaction between O atom and SF_x radical[21,26,28] as stated above. A decrease in the ratio between F and O atom concentration (I_F/I_O) from 0.75 to 0.4 is observed as the oxygen flow rate increases from 2.5 sccm to 20 sccm as shown in Fig. 5.

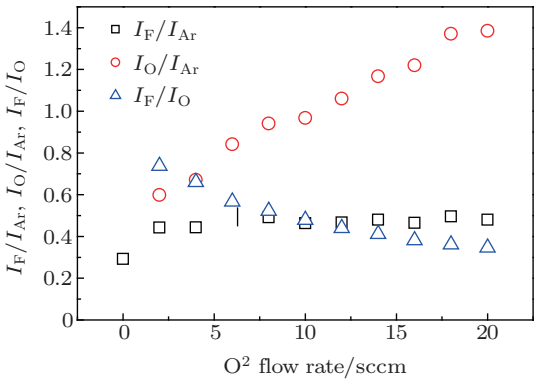


Fig. 5. (color online) Variations of actinometry signals I_F/I_{Ar}, I_O/I_{Ar}, and I_F/I_O with the O_2 flow rate in $SF_6/O_2/Ar$ discharge at 7.5 mTorr, with the upper and lower electrode power being 300 W and 60 W respectively.

The ratios of I_F/I_{Ar}, I_O/I_{Ar}, and I_F/I_O each are plotted as a function of the discharge pressure of SF_6+10%O_2 plasma in Fig. 6. It can be found that F atom concentration increases monotonically with increasing discharge pressure. However, O atom concentration increases with pressure initially and reaches a maximum at about 22.5 mTorr and then decreases with pressure. [F]/[O] ratio increases significantly with increasing pressure.

The ratios of I_F/I_{Ar}, I_O/I_{Ar}, and I_F/I_O are plotted each as a function of the input power of RF 40.68 MHz in Fig. 7. With increasing input power, I_F/I_{Ar} and I_O/I_{Ar} increase with input power increasing initially, reach maximum at about 200 W and then decrease with further increasing input power. Whilst the ratio of I_F/I_O shows an increase with increasing input power, it keeps constant as the input power is larger than 250 W.

As is well known, effective high frequency input power into plasma will lead to the increase in electron density, and the effective high frequency input power into the electronegative plasma can also cause the electron density to increase as shown in Fig. 4. Different from the case in the electro-positive plasma such as Ar, in the electro-negative SF_6/O_2 plasma, an energetic electron participates in the dissociative attachment process with radical or ion conversion.[29] This process is one of the important sources of negative ion formation. The negative ion density in electro-negative plasma may be larger than electron density,[30] usually experiencing a strong reflection near the sheath edge[31] and entering into the bulk with a high concentration. From this, we attempt to understand the reason for the variations of I_F/I_{Ar} and I_O/I_{Ar} with input power. As input power increases as shown in Fig. 4, electron density will increase, which causes a dissociative electron attachment process of SF_6 and O_2 to strengthen. Furthermore, the increase in electron density makes electrons Maxwellianized,[32] which causes the electron temperature to decrease, thereby strengthening the attachment process of lower energy electrons with radical strong electro-negativity. Therefore, the concentration ratios of I_F/I_{Ar} and I_O/I_{Ar} increase with input power increasing. However, as input power is larger than 250 W, I_F/I_{Ar} and I_O/I_{Ar} each show a slight decrease. The reason for that is not clear.

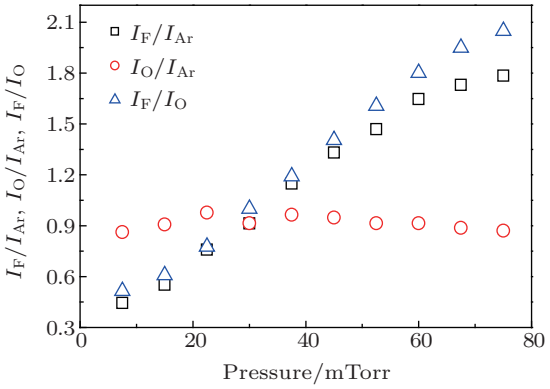


Fig. 6. (color online) Variations of actinometry signals I_F/I_{Ar}, I_O/I_{Ar}, and I_F/I_O with pressure in $SF_6/O_2/Ar$ discharge at 300 W/60 W.

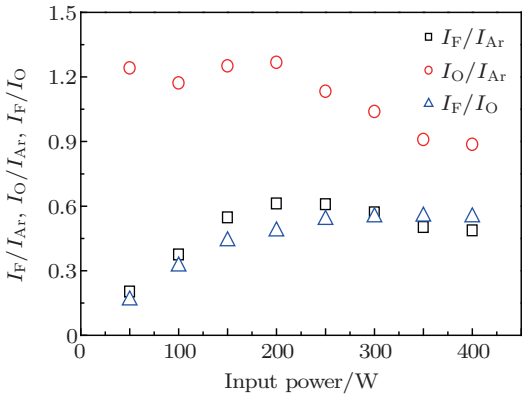


Fig. 7. (color online) Variations of actinometry signals I_F/I_{Ar}, I_O/I_{Ar}, and I_F/I_O with input power in $SF_6/O_2/Ar$ discharge at 7.5 mTorr.

From the influence of discharge parameters on relative emission intensity of F and O radicals in SF_6/O_2 plasma, obtained by using the OES technique, it can be found that the discharge pressure and the flow rate ratio play roles in adjusting the ratio of [F]/[O] in SF_6/O_2 plasma more dominantly than RF input power. In the next subsection, by changing the flow rate ratio and discharge pressure, we will show how the behavior of plasma texturing for mc-silicon changes.

3.3. Plasma texturing of mc-Si with different discharge parameters

As mentioned above, the change of discharge parameters will influence the ratio between F and O concentration in SF_6/O_2 plasma, and thus also influence the texturing structure of the mc-Si surface. In order to elucidate the mechanism of plasma texturing of mc-Si, we carry out a group of experiments in which evolutions of the mc-Si texturing structure with the plasma treatment time are concerned. The typical experimental parameters are as follows: upper and lower electrode power are kept at 300 W and 60 W with gas mixture (SF_6/O_2) flow rates of 45 sccm and 5 sccm and a pressure of 7.5 mTorr, the plasma treatment times are set to be 2, 4, 6, 8, 10 min, respectively. Figures 8(a)–8(d) show surface SEM images of plasma textured multi-crystalline Si for different plasma treatment times, and figures 8(e) and 8(h) show SEM images for the corresponding samples after being immersed in 5% HF solution for 30 s. From the untreated texturing structures in Figs. 8(a)–8(d), we can find that intensive little convexes appear on the mc-Si surface initially, with increasing plasma treatment time, these round convexes grow bigger, with cone-like structures appearing underneath. Analysis of mc-Si surface with raw texturing structure by using X-ray photo-electronic spectroscopy indicates that these convexes are composed of Si–O bonds with less F content. The disappearance of these round convexes on the mc-Si surface due to being immersed into the HF solution and the appearance of cone-like structures as shown in Figs. 8(e) and 8(f) also confirm this point. Therefore, we purpose an evolution process of plasma texturing of mc-Si described as shown in Fig. 9. At the onset of fluoro-oxygen-based plasma, the O atoms in the plasma will initially react randomly with the silicon atoms of the mc-Si surface (step 1 in Fig. 9) and the local oxidation will be further enhanced under the influence of ion bombardment due to the self-bias voltage applied to the lower electrode by 13.56-MHz discharge. Owing to the etching selectivity of about 40:1 of Si and SiO_2 for F atom etchant.[26] Fluorine atom in the plasma preferentially reacts with Si atom rather than SiO_2 to form a volatile SiF_4 into the plasma. That is, the oxidation region just acts as a natural etching barrier, and a cone-like silicon structure with an oxidation hemisphere on the top is shaped (step 2 in Fig. 9). With continuing plasma etching, the size of oxidation hemisphere becomes larger (step 3 in Fig. 9) and the height of the formed cone-like structure becomes deeper with a cone angle of about 35° after being washed in HF acid solution (step 4 in Fig. 9).

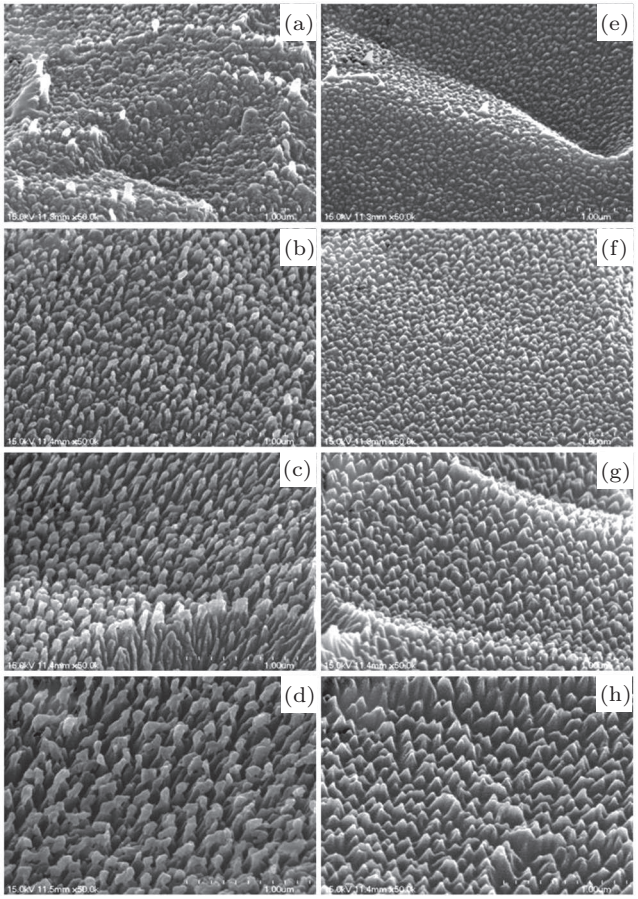


Fig. 8. Surface SEM images of plasma textured mc-Si with plasma treatment times of (a) 2 min, (b) 4 min, (c) 6 min, and (d) 8 min; and (e)–(h) SEM images for the corresponding samples after being immersed in 5% HF solution for 30 s.

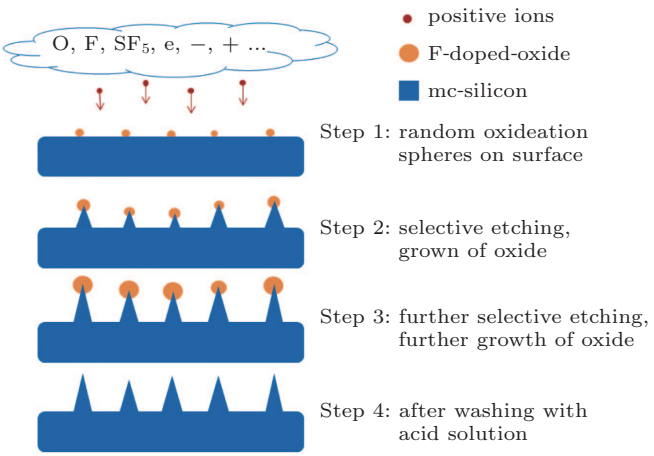


Fig. 9. (color online) A model to explain the evolution mechanism of plasma texturing.

To the naked eye, the mc-Si wafer treated by SF_6/O_2 plasma for an etching time of more than 6 min looks dark.

This indicates a low reflectance for mc-Si treated by SF_6/O_2 plasma. Reflectance values are measured as a function of the wavelength for different plasma treatment times, as shown in Fig. 10. We can see that the reflectivity of the textured mc-Si surface decreases roughly with the averaged depth of the cone-like structure in Fig. 8, because a deeper cone-like structure will by and large reduce the possibility of incident light escaping from the plasma textured surface. A typical photograph plasma textured mc-Si taken from a digital-camera is shown in the inset of Fig. 10. The average reflectance in the wavelength range 30 nm–1200 nm is calculated with respect to the etching time. The average reflectance decreases from 29% for the mc-Si surface with a 2-min plasma treatment to 7.3% for the one with 10 min.

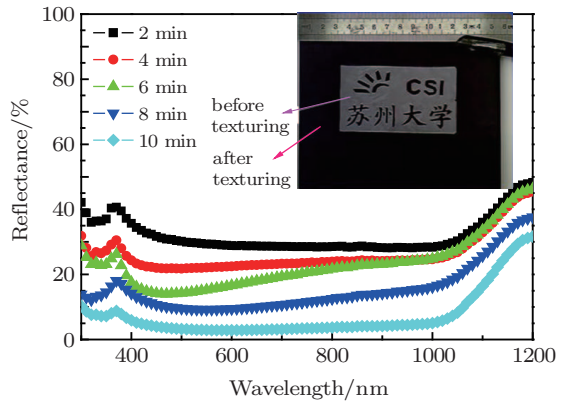


Fig. 10. (color online) Measured reflectance values of mc-Si wafers, each as a function of the wavelength in different surface conditions. Inset: a typical photograph of plasma textured mc-Si taken from a digital-camera.

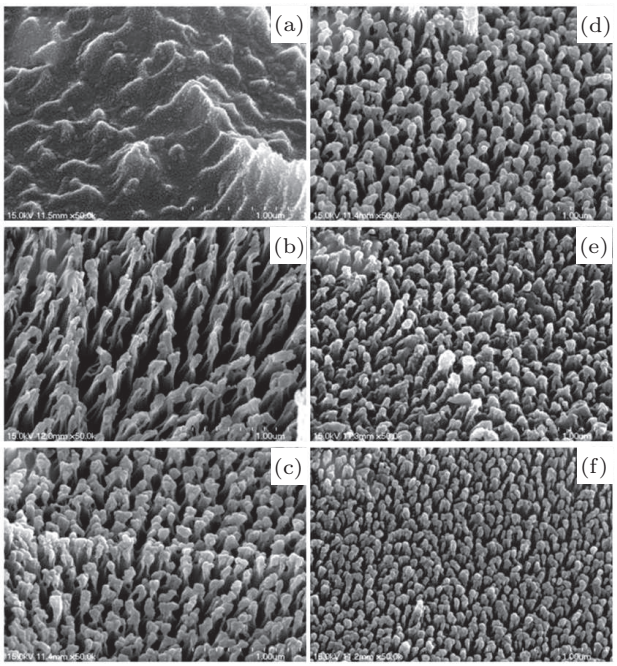


Fig. 11. Surface SEM images of plasma textured mc-Si with plasma treatment times of (a) 0 sccm, (b) 5 sccm, (c) 10 sccm, (d) 15 sccm, (e) 20 sccm, and (f) 25 sccm.

Plasma texturing behaviors of mc-Si with varying O_2 flow rate and pressure are investigated. In order to view the original microstructure of the mc-Si surface, immersion into HF solution for mc-Si after plasma treatment is not carried out. Figure 11 shows the surface SEM images of plasma textured multi-crystalline Si for different flow ratios (SF_6/O_2). Upper electrode power is kept at 300 W, self-bias at −80 V, SF_6 flow rate at 45 sccm, pressure at 7.5 mTorr, and the treatment time at 10 min. It can be found that without O_2 addition, only a few hundred nanometer cone-like structures are found on the mc-Si surface after SF_6 plasma texturing, which may be due to either an original induced surface roughness or a native induced oxidation layer. With increasing the O_2 flow rate, the cone-like structure appears on the mc-Si surface with an irregular oxidation hemisphere located on the tip. The oxidation hemisphere grows bigger first and then smaller after the O_2 flow rate has reached 15 sccm. However, further O_2 addition causes the cone-like structures to be denser and to each have a smaller height. These surface texturing variations are attributed mainly to the competition between the O-radical surface passivation and F-radical surface etching in the SF_6/O_2 plasma as stated before.

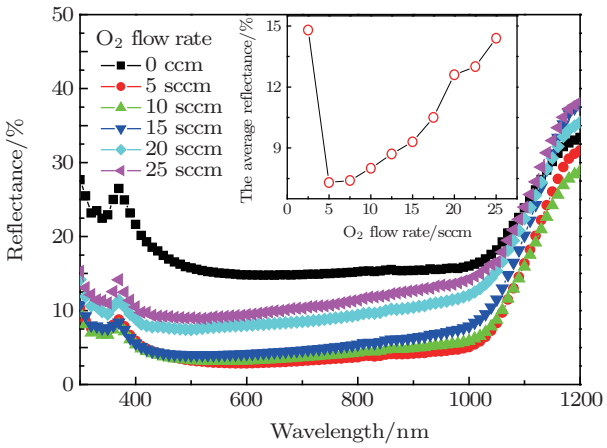


Fig. 12. (color online) Curves of measured reflectance of mc-Si wafers versus wavelength with different O_2 flow rates as a function of the wavelength. Inset: the averaged reflectance of mc-Si wafers with different O_2 flow rates.

Micro-structural variations of these cone-like structures strongly influence their optical reflectivity values. The measured reflectance curves of mc-Si wafers with different O_2 flow rates, each as a function of the wavelength are shown in Fig. 12. The averaged surface reflectance decreases initially, and then increases with increasing O_2 flow rate, as shown in the inset of Fig. 12. Additionally, O_2 addition causes an increase in number density (N) and a decrease in the average height (H) for each of the cone-like structures, as shown in Fig. 13. If taking the product of the number density and the height of a cone-like structure, to a certain extent, we find that the product curve (as shown in the inset of Fig. 13) is similar to the one of average reflectance against O_2 addition. That

is to say, optical reflectance of the textured mc-Si surface is determined by not only the cone-like structure number density but also its height. The smaller the product of $N*H$, the smaller the optical reflectance. For textured mc-Si with lower optical reflectance, obviously, it is necessary to adjust the ratio between F and O radicals in the plasma, thereby achieving a lower number density and optimal height of the cone-like structure. In our experiments, the lowest reflectance of about 7.3% for mc-silicon surface texturing is obtained at an O_2 addition of 10% with a [F]/[O] ratio of 0.5 and an electron density of 6.9×10^9 cm^{-3}.

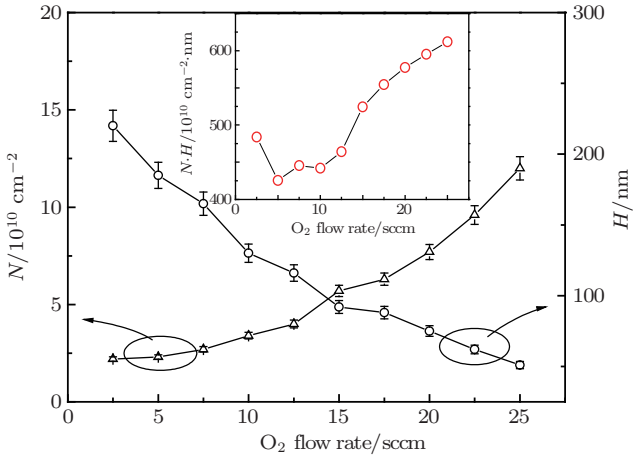


Fig. 13. (color online) Measured cone structure density and the average height of a cone structure each as a function of the O_2 flow rate. Inset shows the product of number density and the height of cone-like structure ($N*H$) as a function of the O_2 flow rate.

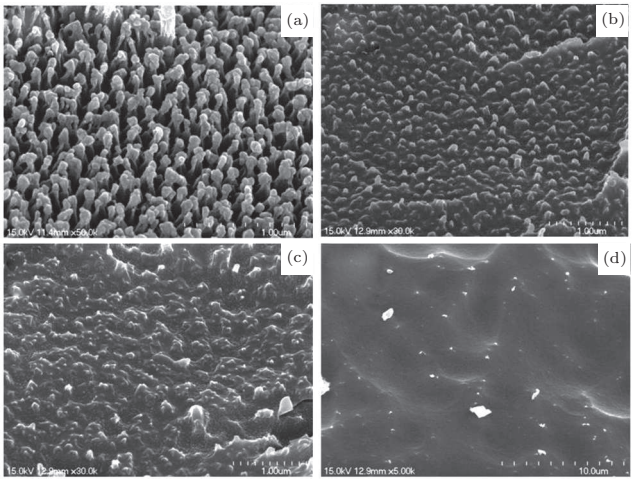


Fig. 14. Surface SEM images of plasma textured multi-crystalline Si at different working pressures: (a) 7.5 mTorr, (b) 22.5 mTorr, (c) 37.5 mTorr, (d) 75 mTorr.

Besides O_2 addition into SF_6, the discharge pressure is also a significant external parameter to adjust the F/O ratio in the plasma. Our experimental results show that mc-Si surface texturing occurs only in a small range of working pressure ($P < 22.5$ mTorr). Out of the range, no cone-like structure forms on the mc-Si surface. Figure 14 shows surface SEM images of plasma textured mc-Si for different working pressures. When the pressure is larger than 22.5 mTorr, sparse cone-like structures with small size are observed. To the naked eye, the silicon wafer textured at less than 22.5 mTorr looks grey. For the pressure at 37.5 mTorr, cone-like structures are sparser. Up to 75 mTorr, the silicon wafer surface is very smooth without any microstructures. As seen previously (Fig. 6 in Section 3), the region for $P < 22.5$ mTorr corresponds to [F]/[O]< 0.8, $n_e > 6.3 \times 10^9$ cm^{-3}. With increasing pressure, the [F]/[O] ratio increases significantly, and the large number of fluorine atoms leads to the enhanced etching. This means that compared with passivation, etching of F atoms is dominated over with increasing pressure.

4. Conclusions

The plasma texturing is performed on multi-crystalline silicon solar cells in a dual-frequency excited capacitively coupled plasma (DF-CCP) reactor using an SF_6/O_2 gas mixture. With the help of optical emission spectroscopy (OES) and a hairpin resonance probe (HRP), the influences of the plasma characteristics on mc-silicon surface plasma texturing are investigated with different flow rate ratios, pressures, and radio-frequency input powers, and suitable conditions are suggested for the application to mc-silicon solar cells. The HRP results show that the electron density continuously decreases with the increase of the O_2 flow rate in SF_6 discharge. The OES results show that the [F]/[O] ratio is a decisive factor of plasma texturing, which is influenced by the change of discharge parameters in SF_6/O_2 plasma and thus affects the texturing structure of the mc-Si surface. Our experiments have shown a suitable plasma texturing of mc-silicon only in a narrow plasma parameter window, where n_e must be larger than 6.3×10^9 cm^{-3} and the ratio of spectral intensity of F and O atom ([F]/[O]) in the plasma must be less than 0.8 and more than 0.3. Out of this range, no cone-like structure is formed on the mc-silicon surface. The investigation process will support valuable information in industrial plasma texturing development of mc-Si in the future.

References

[1] Inomata Y, Fukui K and Shirasawa K 1997 *Sol. Energy Mater. Sol. Cells* **48** 237
[2] Fukui K, Okada K, Inomata Y, Takahashi H, Fujii S, Fukawa Y and Shirasawa K 1997 *Sol. Energy Mater. Sol. Cells* **48** 219
[3] Shirasawa K, Fukui K, Okada K, Inomata Y, Takahashi H and Fujii S 1997 14*th EC Photovoltaic Solar Energy Conference*, Barcelona, Spain, pp. 384–387
[4] Ruby D S, Zaidi S H, Narayanan S, Damiani B M and Rohatgi A 2002 *Sol. Energy Mater. Sol. Cells* **74** 133
[5] Yoo J, Kim K, Thamilselvan M, Lakshminarayn N, Kim Y K, Lee J, Yoo K J and Yi J 2008 *J. Phys. D: Appl. Phys.* **41** 125205
[6] Yoo J 2010 *Solar Energy* **84** 730
[7] Yoo J, Yu G and Yi J 2011 *Sol. Energy Mater. Sol. Cells* **95** 2
[8] Liang L, Nakamura K and Sugai H 2011 *Appl. Phys. Express* **4** 066101
[9] Piejak R B, Al- Kuzee J and Braithwaite N S 2005 *Plasma Sources Sci. Technol.* **14** 734

[10] Karkari S K, Gaman C, Ellingboe A R, Swindells I and Bradley J W 2007 *Meas. Sci. Technol.* **18** 2649
[11] Stenzel R L 1976 *Rev. Sci. Instrum.* **47** 603
[12] Piejak R B, Godyak V A, Garner R, Alexandrovich B M and Sternberg N 2004 *J. Appl. Phys.* **95** 3785
[13] Hebner G A and Abraham I C 2001 *J. Appl. Phys.* **90** 4929
[14] Hebner G A and Abraham I C 2002 *J. Appl. Phys.* **91** 9539
[15] Curley G A, Maric D, Booth J P, Corr C S, Chabert P and Guillon J 2007 *Plasma Sources Sci. Technol.* **16** S87
[16] Coburn J W and Chen M 1980 *J. Appl. Phys.* **51** 3134
[17] Dreyfus R W, Jasinski J M, Walkup R E and Selwyn G S 1985 *Pure Appl. Chem.* **57** 1256
[18] Donnelly V M, Flamm D L, Dautremont-Smith W C and Werder D J 1984 *J. Appl. Phys.* **55** 242
[19] Walkup R E, Saenger K L and Selwyn G S 1986 *J. Chem. Phys.* **84** 2688
[20] Booth J P, Joubert O, Pelletier J and Sadeghi N 1991 *J. Appl. Phys.* **69** 618
[21] Booth J P, Joubert O, Pelletier J and Sadeghi N 1991 *J. Appl. Phys.* **69** 618
[22] Plank N O V, Blauw M A, Drift E W J M and Cheung R 2003 *J. Phys. D: Appl. Phys.* **36** 482
[23] Huang X J, Xin Y, Yuan Q H and Ning Z Y 2008 *Phys. Plasmas* **15** 073501
[24] Sugai H 2005 *Plasma Electronic Engineering* (Beijing: Science Press) p. 61 (in Chinese)
[25] Zou S, Tang Z H, Ji L L, Su X D and Xin Y 2012 *Acta Phys. Sin.* **61** 075204 (in Chinese)
[26] D'Agostino R and Flamm D L 1981 *J. Appl. Phys.* **52** 162
[27] Brown M S, Scofield J D and Ganguly B N 2003 *J. Appl. Phys.* **94** 822
[28] Anderson H M, Merson J A and Light R W 1986 *IEEE Trans. Plasma Sci.* **2** 156
[29] Benhenni M and Yousfi M 2012 *Plasma Sources Sci. Technol.* **21** 015014
[30] Tuszewski M and White R R 2002 *Plasma Sources Sci. Technol.* **11** 338
[31] Takizawa K, Kono A and Sasaki K 2007 *Appl. Phys. Lett.* **90** 011503
[32] Flamm D L, Donnelly V M and Mucha J A 1981 *J. Appl. Phys.* **52** 3633